Supplementary Information (SI) for Journal of Materials Chemistry A.

Supplementary Information

Anti-Freezing Flexible Polymer Electrolyte for High-Performance Zinc-Ion Battery

Hyocheol Lee,[1,] Rangaswamy Puttaswamy[1], Le Mong Anh[1], Dukjoon Kim*[1]

[1]School of Chemical Engineering, Sungkyunkwan University, Suwon, Gyeonggi, 16419, Republic of Korea.

[*] Corresponding author: Dukjoon Kim

Tel.: +82 31 290 7250

Fax: +82 31 290 7270

Email address: djkim@skku.edu (D. Kim)

Experimental section

Materials

4,4-bis(4-hydroxyphenyl) valeric acid (HVA), bis(4-fluorophenyl) sulfone (BFS), potassium carbonate (K_2CO_3), N,N'-dicyclohexylcarbodiimide (DCC), and 4-dimethylaminopyridine (DMAP) were purchased from Sigma-Aldrich (Milwaukee, WI, USA). Polyethylene glycol monomethyl ether 2000 (PEG 2000) was purchased from Tokyo Chemical Industry (TCI, Japan). These materials were used to synthesize poly(arylene sulfone ether)-g-polyethylene glycol (PAES-g-PEG). Zinc (II) trifluoromethanesulfonate ($Zn(CF_3SO_3)_2$) was purchased from TCI. Deionized (DI) water and ethylene glycol (EG) were purchased from Samchun Chemicals (Korea). Carbon black (Super P) was provided by Sigma Aldrich and used to prepare cathodes for the ZIBs. Dimethylformamide (DMF, >99.0%), isopropanol (IPA, 99.5%), tetrahydrofuran (THF, 99.5%), 1-methyl-2-pyrrolidone (NMP, 99.5%), and hydrochloric acid (HCl) were purchased as reagents from Samchun Chemicals (Korea).

Synthesis of PAES-g-PEG

As shown in **Scheme S1**, a mixture of HVA (8.58 g, 0.03 mol), BFS (10.5 g, 0.03 mol), K_2CO_3 (10.36 g, 0.075 mol) in toluene (120 mL), and DMSO (120 mL) was stirred in a 500 mL four-neck round bottom flask for 2 days at 172.5 °C to synthesize PAES-COOK. After the reaction was completed, THF (100 mL) and HCl (30 mL) were added to the reactor to convert from PAES-COOK to PAES-COOH, and the polymer mass was stirred for several hours until it dissolved. The PAES-COOH solution was then precipitated in 1.5 L of IPA, and the obtained PAES-COOH solid was washed several times with DI water. Finally, the PAES-COOH solid was dried in a 60 °C vacuum oven for 24 h to obtain pure PAES. The yield of PAES-COOH was > 90%. To graft PEG into the PAES-COOH main chain, PAES-COOH (14.0 g, 0.028 mol) and PEG (61.6 g, 0.0308 mol) were dissolved in DMF (300 mL) at 83 °C. After 1 h, DCC (9.24

g, 0.0448 mol) and DMAP (0.55 g, 0.00448 mol) were added to the reactor and the reaction occurred at 80 °C for 2 days. After the reaction was complete, the product was precipitated in 1.5 L of ether, washed with DI water, and filtered several times. The solid PAES-g-PEG was dried under vacuum at 60 °C for 1 day to obtain pure PAES-g-PEG.

Preparation of SPEs using PAES-g-PEG

H_2O, EG, and the H_2O/EG solution were added to the SPE. PAES-g-PEG (0.3 g), $Zn(CF_3SO_3)_2$ (52, 104, and 156 mg; 0.5, 1.0, and 1.5 M), and the H_2O/EG solution (0.3 g) were dissolved in THF (2 mL), and mixed for 24 h. After that, the polymer solution was cast onto a PTFE Petri dish and dried at 40 °C for 30 mins. The thickness of SPEs was controlled to be in the range of 100-110 μm. The SPEs were named based on the amount of $Zn(CF_3SO_3)_2$ added to the membrane (nn M Zn-additive-SPE; nn = 0.5, 1.0, and 1.5). At concentrations higher than 1.5 M, the polymer electrolyte membrane did not form.

Synthesis of $V_{10}O_{24}\cdot nH_2O$@rGO composite

The $V_{10}O_{24}\cdot nH_2O$@rGO composite was synthesized following a previously reported method with some modifications.[1] Briefly, 1 g of commercial V_2O_5 powder and 1 g of glucose were dispersed in 30 mL of distilled H_2O and refluxed at 100 °C under vigorous stirring. The reaction continued for 2 h, during which the solution gradually changed from yellow to light green. Once the solution attained a light green color, 200 mg of graphene oxide (GO) suspension (prepared by dispersing GO in 50 mL of H_2O and sonicating for 30 minutes) was added. The mixture was stirred thoroughly at 100 °C for 12 h to ensure uniform incorporation. The resulting product was washed multiple times with an H_2O/ethanol mixture (1:1 = v/v) via centrifugation (5 minutes per cycle) to eliminate impurities and remove free-standing rGO sheets. Finally, the purified product was dried at 70 °C for 10 h.

Preparation of vanadium cathodes for ZIBs and cell assembly

To prepare the cathodes for the ZIBs, $V_{10}O_{24}\cdot nH_2O$@rGO (70 wt%), Super P (20 wt%), and PAES-g-PEG (10 wt%) as a binder were mixed in a 20 mL vial, and NMP (500 mg) was slowly added to the mixture. This mixture was sonicated for 2 h. After mixing was completed, the slurry was cast onto carbon paper (diameter (θ) of 14 mm, MTI Korea) and dried in a vacuum at 80 °C overnight. The mass loading of the vanadium cathode was around 0.9-1.0 mg cm^{-2} and 3.0 mg cm^{-2}. The electrochemical characterization was performed using CR2032 coin cells, with Zn-metal as the anode (thickness (t) = 0.05 mm, MTI Korea).

Characterization of SPEs

Chemical properties of SPEs

The chemical structures of the polymeric materials were identified using ^{1}H nuclear magnetic resonance spectroscopy (^{1}H-NMR) (Oxford 300 NMR, VARIAN, USA) and a Fourier transform infrared spectrometer (FT-IR) (Secondary Nicolet iS10, Thermo Fisher Scientific, USA).

Phase separation behavior of SPEs

The phase separation behavior was evaluated using the small-angle X-ray scattering (SAXS) (SAXSess MC2, Anton Paar, Austria), and the dimension of the PEG domains (d) was calculated from the scattering vector (q) obtained by the SAXS.

$$d\ (nm) = \frac{2\pi}{q} \tag{1}$$

Mechanical and thermal properties of SPEs

The mechanical properties of the SPEs were investigated using a universal tensile machine (UTM) (LR30K Plus, Lloyd Instruments, Republic of Korea). The SPEs were cut into specimens with dimensions of 1 cm x 4 cm x 100 μm before measurement. The thermal properties of SPEs were evaluated using differential scanning calorimetry (DSC) (DSC-Q20, Seiko, Japan) and thermogravimetric analysis (TGA) (TG/DTA7300, Hitachi, Japan). The DSC measurements were conducted at a scanning rate of 5 °C min^{-1} in the temperature range from -60 °C to 200 °C. The TGA measurements were also conducted at a scanning rate of 10 °C min^{-1} in a temperature range from 20 °C to 600 °C.

Electrochemical characterizations of SPEs

A CR2032 coin cell was used to measure the electrochemical properties. Additionally, a stainless steel (SS) SS|SPE|SS symmetric cell was employed to measure the ionic conductivity through electrochemical impedance spectroscopy (EIS) analysis. The Zn ion conductivity (σ) was calculated using the following equation.

$$\sigma = \frac{t}{A \times R} \tag{2}$$

where t is the thickness of the SPE, A is the area of the SPE, and R is the bulk resistance of the SPE at various temperatures ranging from -40 °C to 80 °C. R was measured using the potential electrochemical impedance spectroscopy (PEIS) method (VMP3, Biologic Science Instrument, France) in the frequency range from 1 Hz to 10^5 Hz, and the data were analyzed using the Zfit software. Additionally, the thermal activation energy (E_A) was calculated according to equation (4) based on the Arrhenius model.

$$\sigma = Ae^{\frac{-E_A}{RT}} \tag{3}$$

where A is the Arrhenius constant, R is the gas constant (8.31 J K^{-1} mol^{-1}), and T is the temperature. The real (*ε'*) and imaginary (*ε")* parts of the dielectric permittivity were determined using the real (Z') and imaginary (Z") impedance values, respectively, were calculated as follows:

$$\varepsilon' = \frac{Z''}{\omega C_0(Z'^2 + Z''^2)} \tag{4}$$

$$\varepsilon'' = \frac{Z'}{\omega C_0(Z'^2 + Z''^2)} \tag{5}$$

where Z’ and Z” represent the real and imaginary parts of the impedance, respectively; ω is the angular frequency ($\omega = 2\pi f$, where f is frequency); and C_0 is the capacitance of a vacuum ($C_0 = \frac{\varepsilon_0 A}{t}$, where A and t are the area and thickness of the SPE, respectively, and ε_0 is the vacuum permittivity of 8.854×10^{-12} F m^{-1}).

To determine the Zn ion transference number ($t_{Zn}{}^{2+}$), a symmetric coin cell was assembled with the configuration Zn|SPE|Zn. Before the chronoamperometry (CA) test, EIS was conducted to determine the initial interfacial resistance. After the CA measurement, a subsequent EIS analysis was performed to evaluate the final resistance. The transference number ($t_{Zn}{}^{2+}$) was calculated using the data from both the CA and EIS measurements and was determined through Equation 6.

$$t_{Zn}{}^{2+} = \frac{I_S\,(\Delta V - I_0 R_0)}{I_0\,(\Delta V - I_S R_S)} \tag{6}$$

Where I_0 is the initial current, I_s is the steady-state current measured from the CA profile, ΔV is the applied voltage (20 mV), and R_0 and R_s are the interfacial resistance before and after the CA measurement, respectively.

For the electrochemical stability of SPEs, the linear sweep voltammetry (LSV) and Zn stripping/plating cycling tests were investigated. The LSV tests were conducted from 0 to 5.0 V at a scan rate of 0.5 mV s^{-1} using an asymmetric SS|SPE|Zn cell. Additionally, to analyze the long-term stability and electrochemical performance of the membrane, Zn stripping/plating cycling experiments were conducted using a Zn|SPE|Zn symmetric cell. For the long-term stripping/plating cycling test, the experiment was performed at 0.1 mA cm^{-2} for 1700 h at RT and 400 h at -20 °C under the same current density. Additionally, to determine the critical current density, cycling tests were conducted at various current densities of 0.1, 0.25, 0.5, 1.0, and 2.0 mA cm^{-2}, with each current density subjected to 50 cycles of repeated testing. Images of the Zn-metal surface before and after the stripping/plating cycling tests were obtained using field emission scanning electron microscopy (FESEM) (JSM-7600F, Japan).

Electrochemical characterizations of ZIB

The performance of ZIBs was investigated through galvanostatic cycling tests using a VMP3 (Bio-Logic Science, France) and a battery cycler (WBCS3000S, Wonatech, Korea) by measuring the cyclic voltammetry (CV), rate capability, and cycling performance. To determine the operating range and kinetics of the ZIB cells, CV was evaluated at scan rates of 0.2, 0.4, 0.6, 0.8, and 1.0 mV s^{-1} within a voltage range of 0.2 to 1.6 V. The rate capability and cycling performance were measured to assess the long-term stability of ZIB cells at various current densities of 0.05-20.0 A g^{-1} within the same voltage range. The electrochemical investigation at low temperatures was conducted in a constant temperature chamber (DICTH-150SL5, DIC, Republic of Korea).

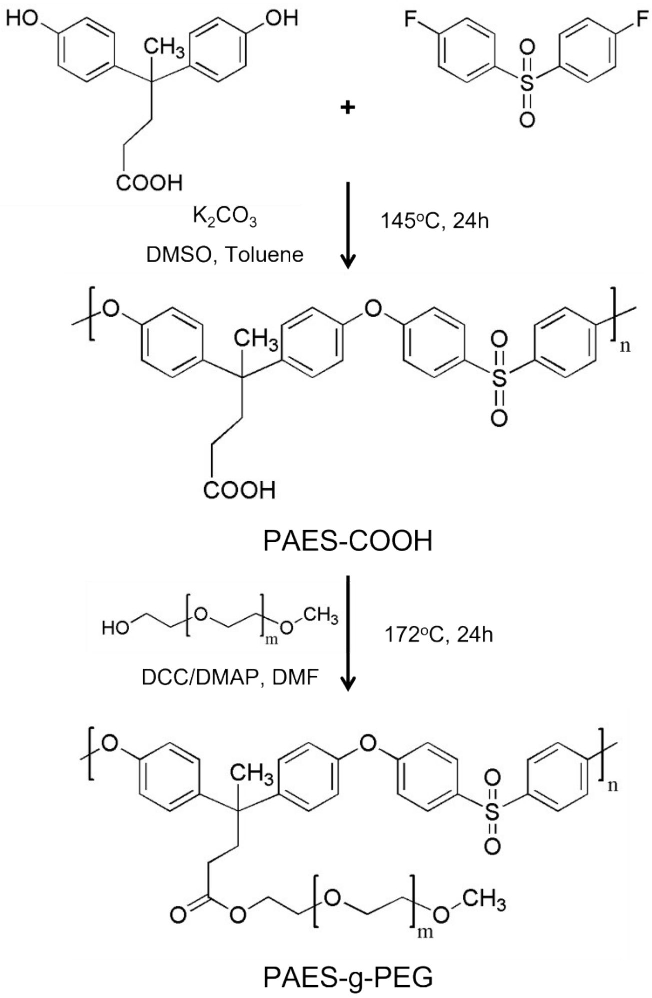

Scheme S1. Synthesis route of PAES-COOH and PAES-g-PEG.

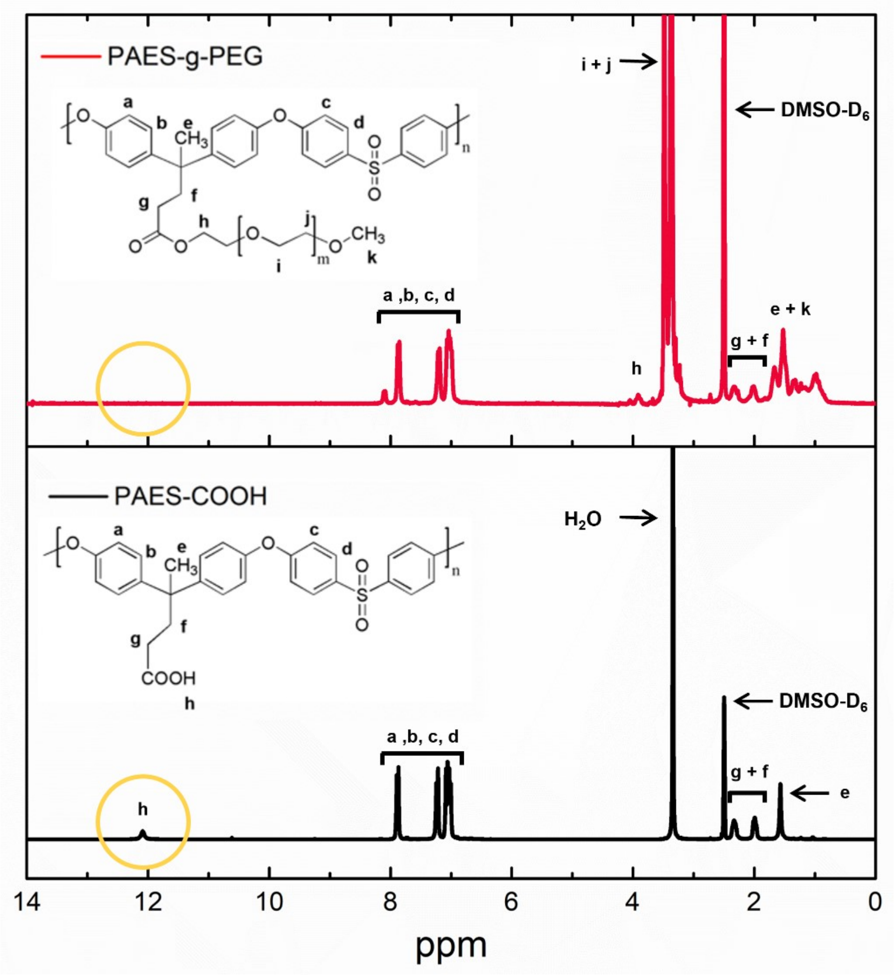

Figure S1. ^{1}H-NMR spectra of PAES-COOH and PAES-g-PEG.

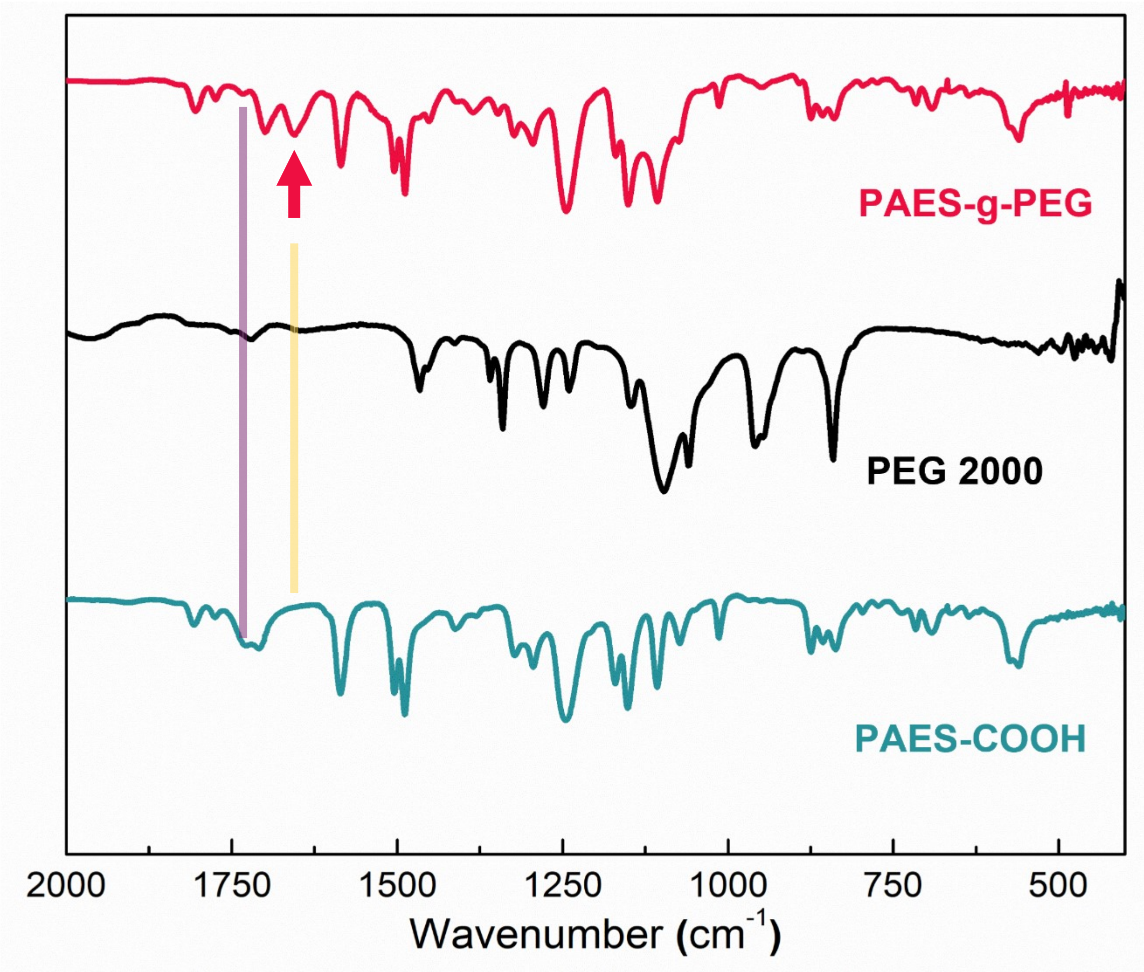

Figure S2. FT-IR spectra of PAES-COOH, PEG2000, and PAES-g-PEG.

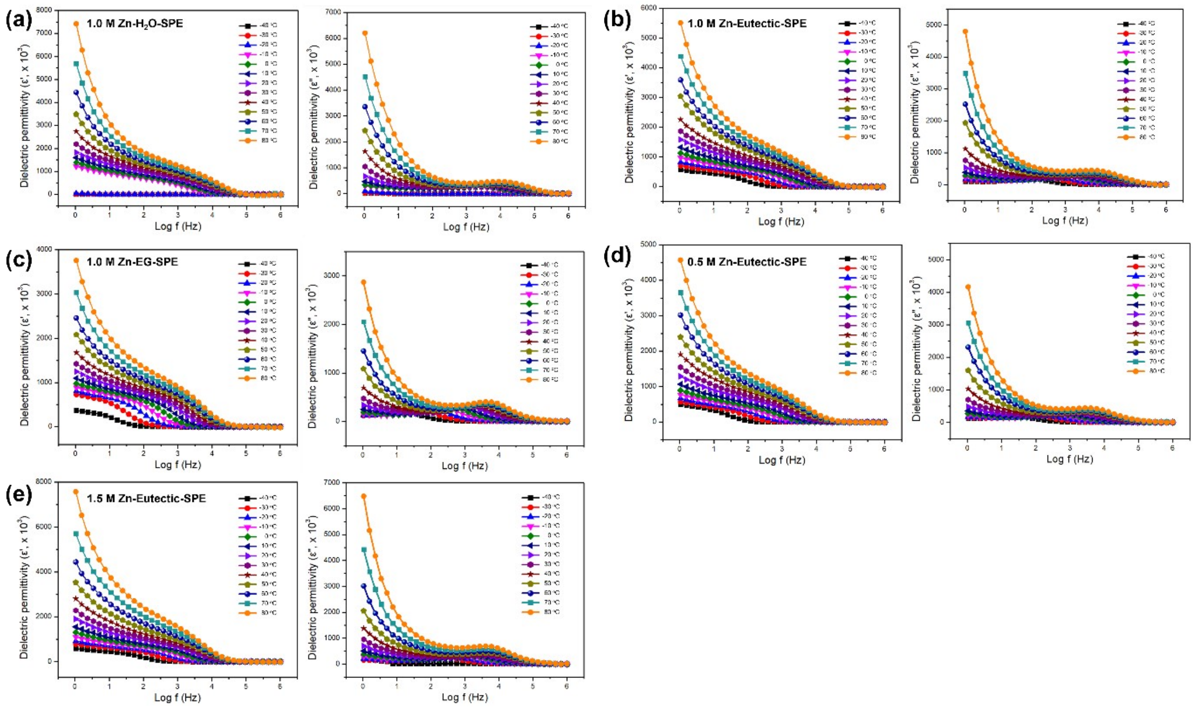

Figure S3. Dielectric permittivity for (a) 1.0 M Zn-H$_2$O-SPE, (b) 1.0 M Zn-Eutectic-SPE, (c) 1.0 M Zn-EG-SPE, (d) 0.5 M Zn-Eutectic-SPE, and (e) 1.5 M Zn-Eutectic-SPE.

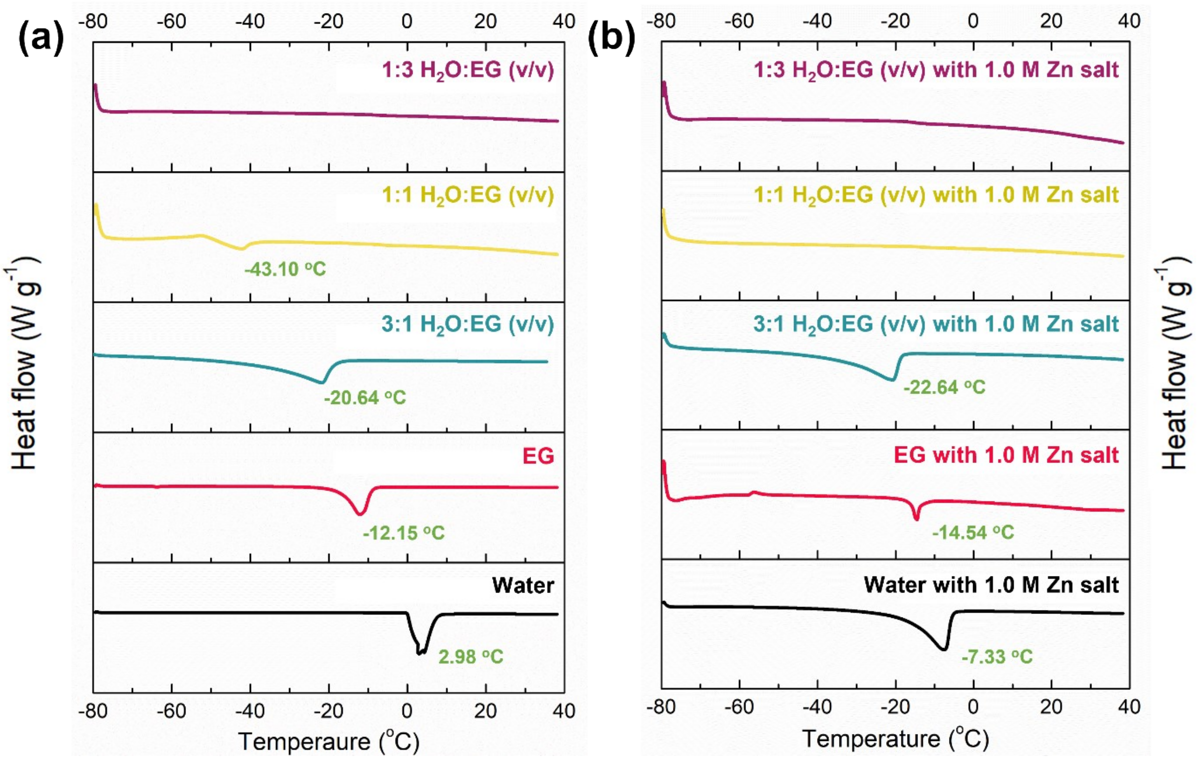

Figure S4. DSC thermograms: (a) the pure solution and (b) the solution containing 1.0 M of Zn salt.

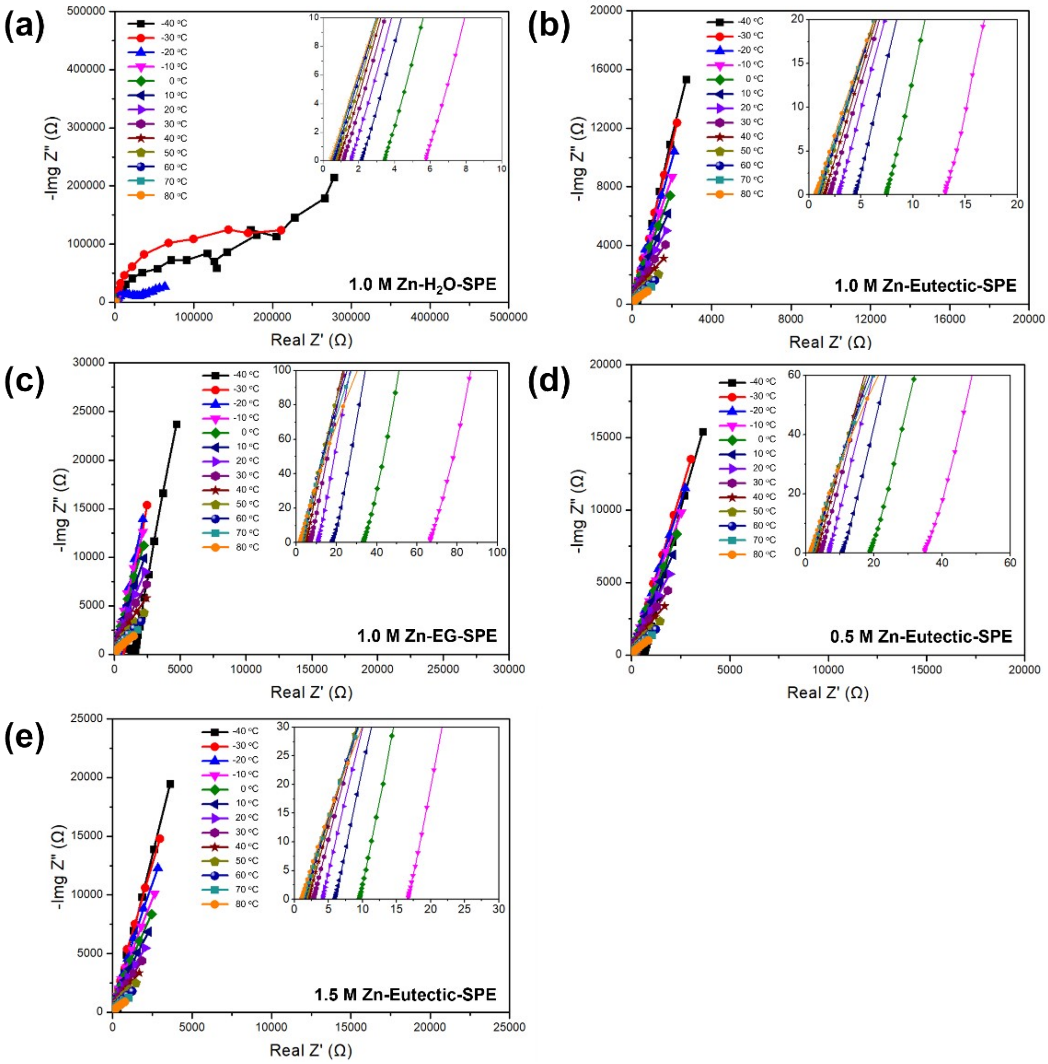

Figure S5. Nyquist plots at various temperatures for (a) 1.0 M Zn-H$_2$O-SPE, (b) 1.0 M Zn-Eutectic-SPE, (c) 1.0 M Zn-EG-SPE, (d) 0.5 M Zn-Eutectic-SPE, and (e) 1.5 M Zn-Eutectic-SPE.

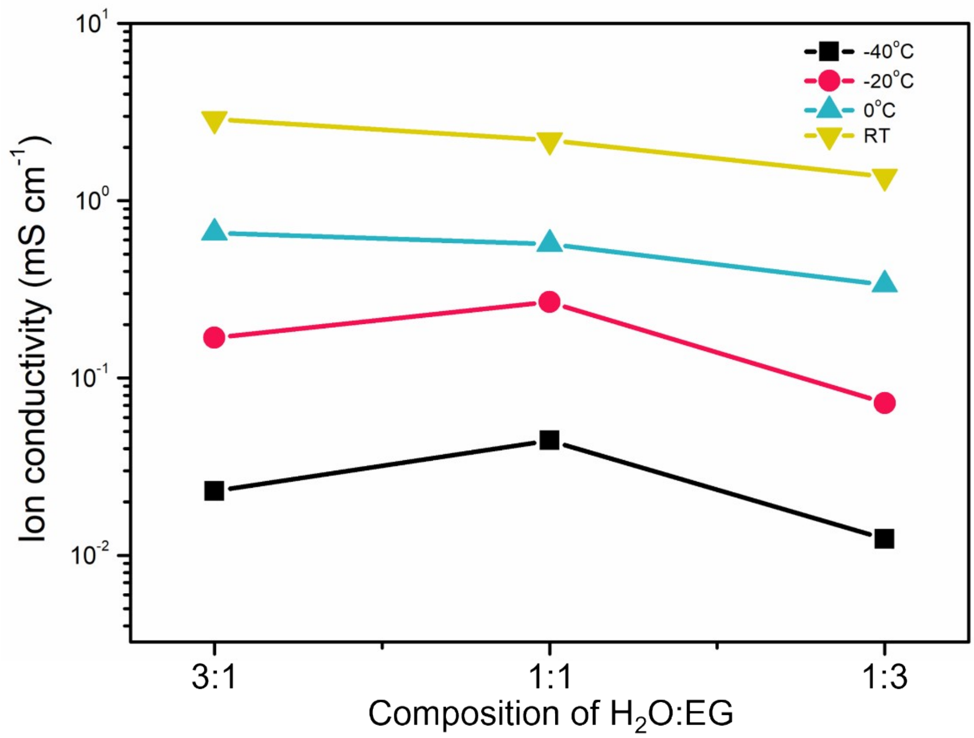

Figure S6. Ionic conductivity of SPEs with 3:1, 1:1, and 1:3 H_2O:EG (v/v) solution at different temperatures.

To enable a fair comparison with liquid electrolyte-based cells from reference studies, we fabricated the SPE with a thickness comparable to that of separators commonly used in aqueous zinc-ion batteries. In the liquid electrolyte-based cells, a glass fiber membrane (GF/C) was employed as the separator with a thickness of 111 μm. The ionic conductivity and dielectric permittivity of both systems were measured and compared, as shown in **Table S1**. As expected, the liquid electrolyte-based cell exhibited higher ionic conductivity and dielectric permittivity due to its inherently greater ion mobility and freer molecular motion. In contrast, the SPE showed lower conductivity butt offered significant advantages in mechanical strength and electrochemical stability, contributing to enhanced long-term battery performance and safer operation. We believe these findings provide a comprehensive understanding of the trade-offs between the two systems and highlight the practical benefits of using SPE in ZIBs.

Table S1. Comparison of Zn-ion conductivity and dielectric permittivity between 1.0 M Zn-Eutectic-SPE and GF/C separator.

Sample	Thickness (um)	Ion conductivity at RT (mS cm^{-1})	Dielectric permittivity (ε', x 10^3)
1.0 M Zn-Eutectic-SPE	100-110	2.32	3065
GF/C separator	111	8.00	3867

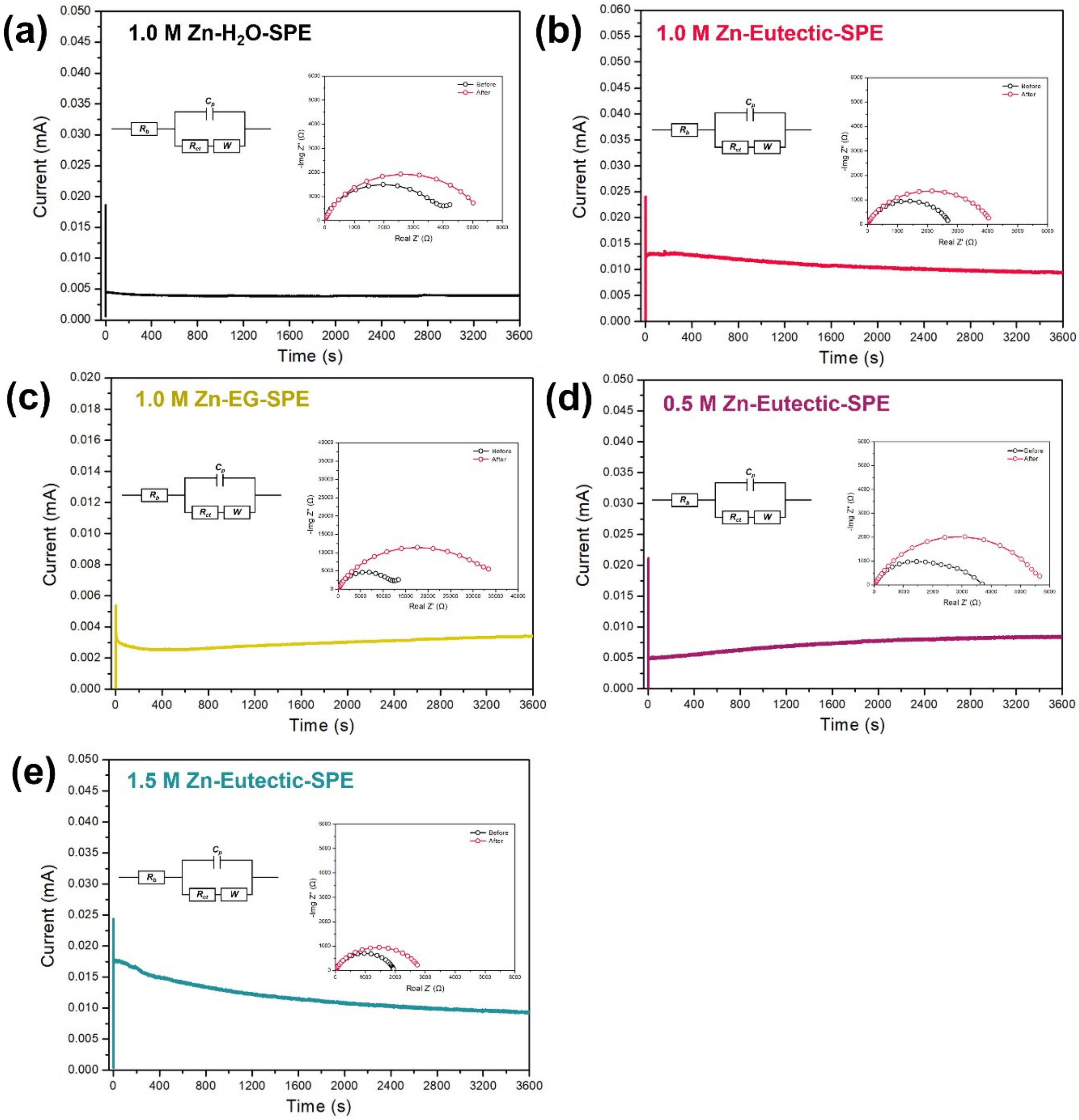

Figure S7. I-T curves and EIS spectra for (a) 1.0 M Zn-H_2O-SPE, (b) 1.0 M Zn-Eutectic-SPE, (c) 1.0 M Zn-EG-SPE, (d) 0.5 M Zn-Eutectic-SPE, and (e) 1.5 M Zn-Eutectic-SPE.

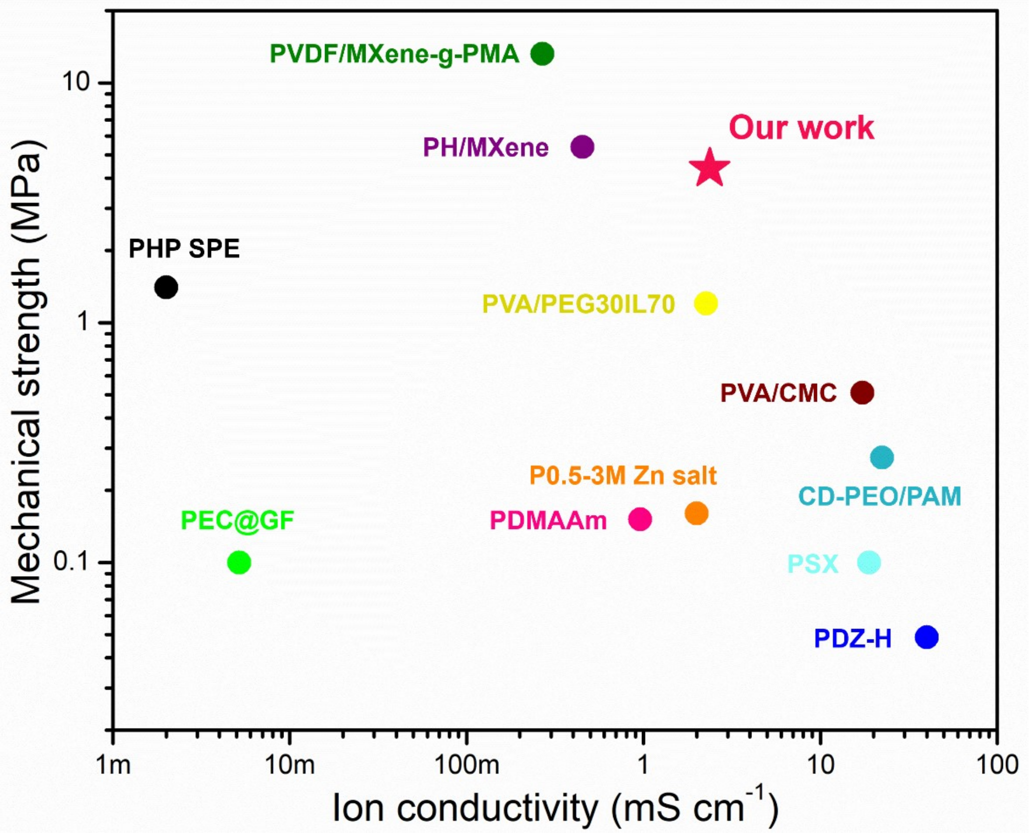

Figure S8. Comparison of ionic conductivity and mechanical strength of our polymer electrolyte with other reported studies.[2-12]

Table S2. Ionic conductivity and mechanical strength values in our work compared to other reported results.

Polymer electrolyte	**Ionic conductivity [mS cm^{-1}]**	**Mechanical Strength$^{(1)}$ [MPa]**	**Ref**
PEC@GF-30%	0.005183	0.1	[2]
PHP SPE	0.002	1.4	[3]
PVA/CMC	17.3	0.51	[4]
P0.5-3M Zn salt	2	0.16	[5]
PSX	18.86	0.1	[6]
CD-PEO/PAM	22.4	0.2733	[7]
PH/MXene SPE	0.452	5.39	[8]
PDZ-H	40	0.0488	[9]
PDMAAm	0.96	0.151	[10]
PVA/PEG30/IL70	2.2264	1.20	[11]
PVDF/MXene-g-PMA	0.269	13.2	[12]
1.0 M Zn-Eutectic-SPE	**2.46**	**4.18**	**Present work**

(1) Mechanical strength is a tensile strength

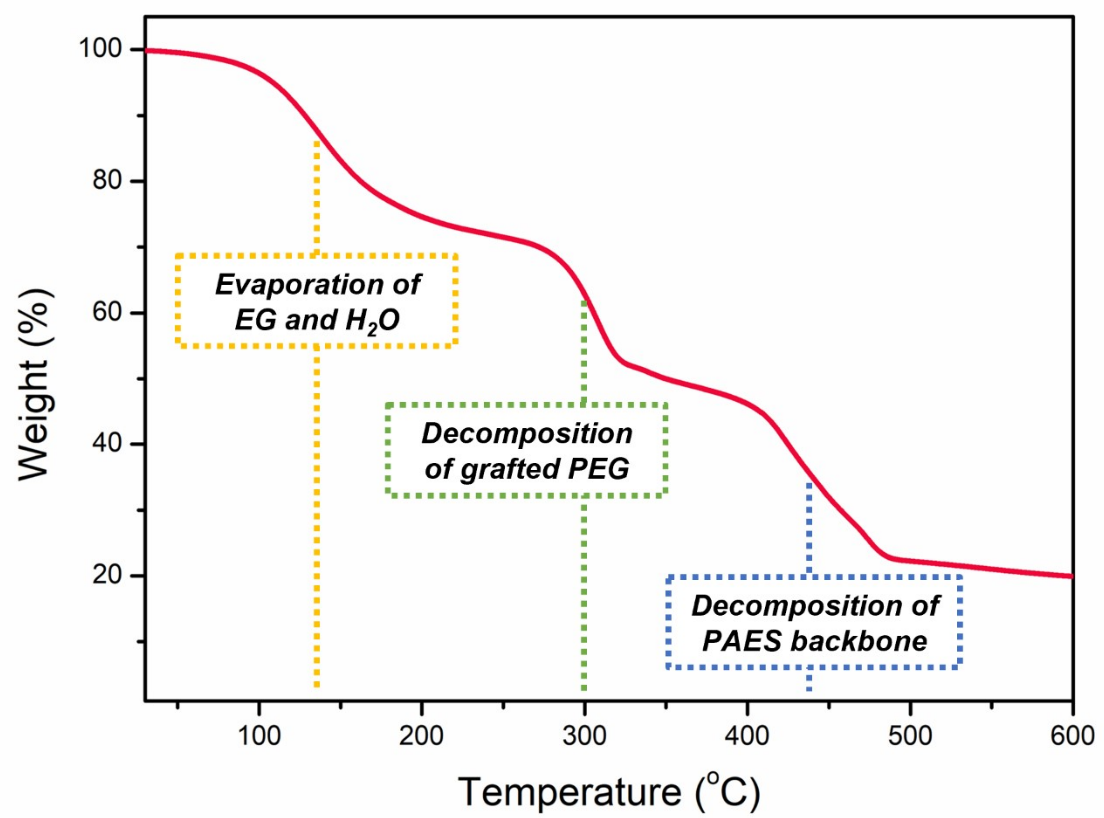

Figure S9. TGA profile of the 1.0 M Zn-Eutectic-SPE.

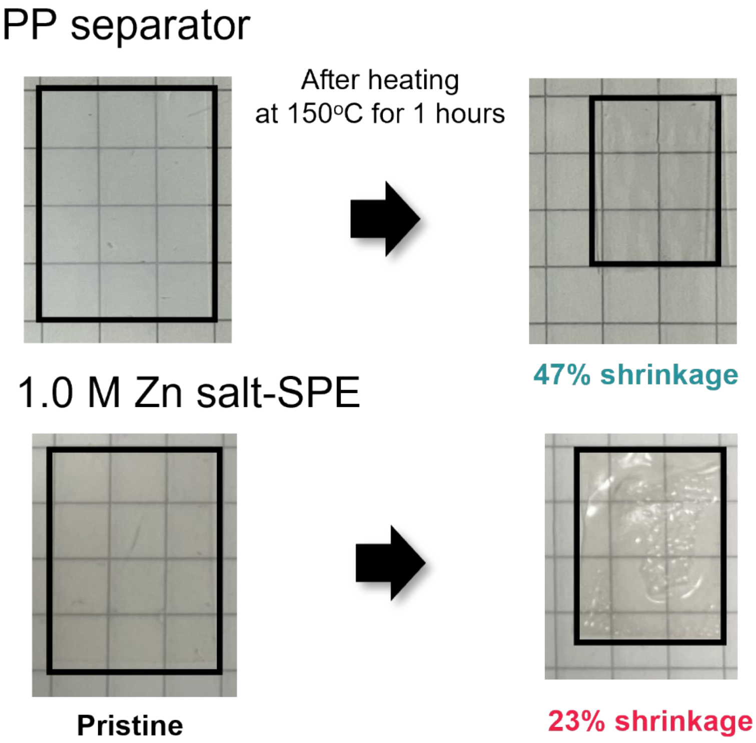

Figure S10. Thermal shrinkage behavior of the conventional polypropylene (PP) separator and 1.0 M Zn-Eutectic-SPE.

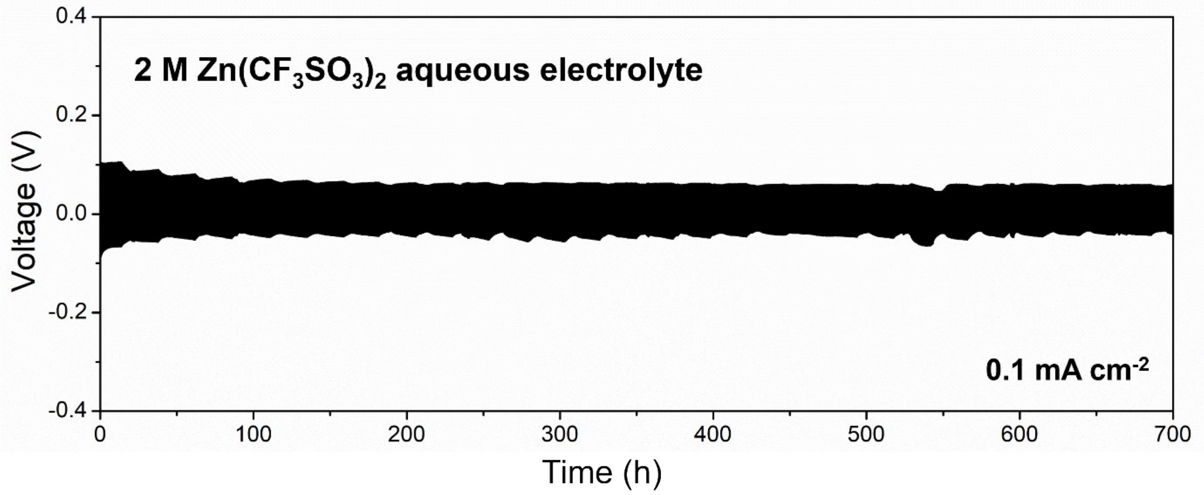

Figure S11. Zn Stripping/plating cycling of Zn symmetric cell at 0.1 mA cm^{-2} with 2 M $Zn(CF_3SO_3)_2$ aqueous electrolyte.

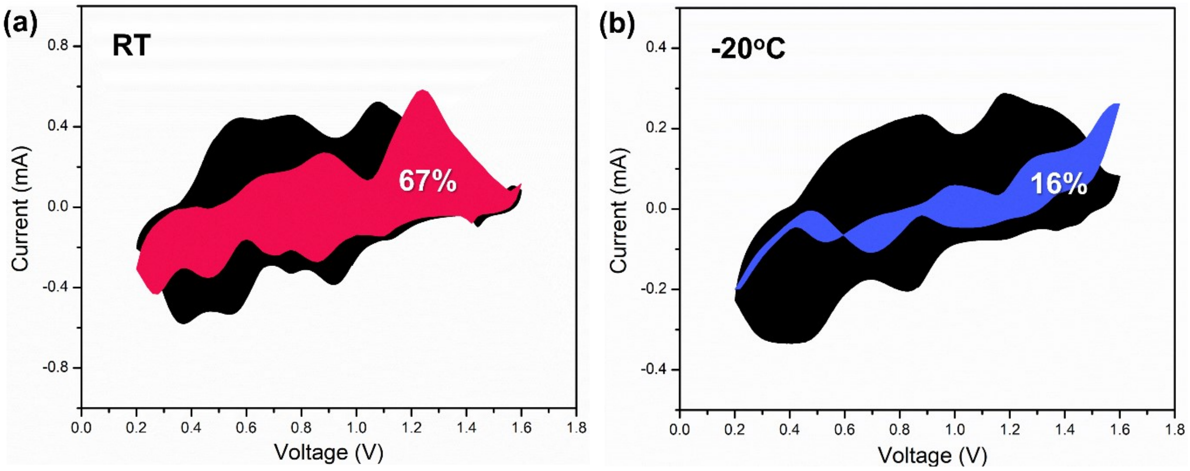

Figure S12. Integrated surface-controlled and diffusion-controlled current contribution at a scan rate of 0.2 mV s^{-1} at (a) RT and (b) -20 °C.

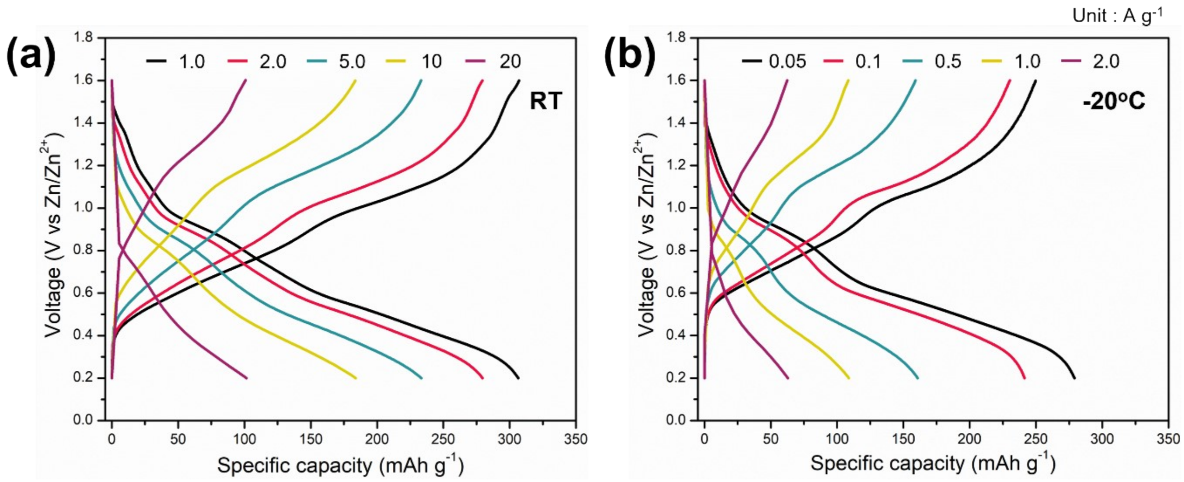

Figure S13. Charge/discharge profiles of Zn|SPE|$V_{10}O_{24}\cdot nH_2O$@rGO cells at different current densities: at (a) RT and (b) -20 ℃.

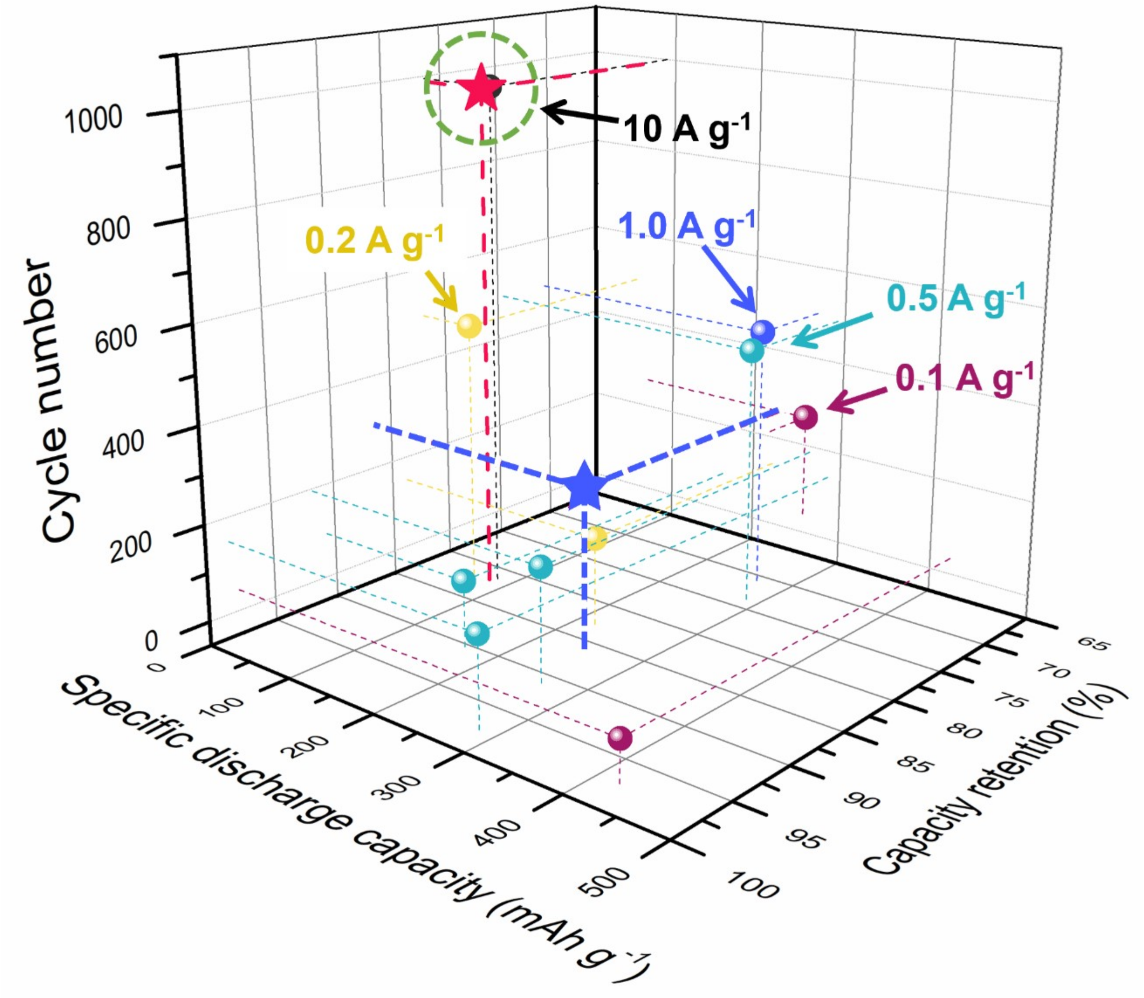

Figure S14. Comparison of the performance of a vanadium cathode|SPE|Zn cell based on the 1.0 M Zn-Eutectic-SPE with those of other recently reported electrolytes[5-8,11,13-17] in terms of the cycle number, specific discharge capacity, and capacity retention.

Table S3. Comparison of ZIB cycling performance in our work and other reported results.

Polymer electrolyte	**Specific discharging capacity after cycling [mAh g^{-1}]**	**Capacity retention [%]**	**Cycle number**	**Current density [A g^{-1}]**	**Ref**
P0.5-3M Zn salt	300	75	500	0.5	[5]
PSX	210	60	200	0.1	[6]
CD-PEO/PAM	430.2	98	50	0.1	[7]
PH/MXene SPE	293	98.3	150	0.5	[8]
PVA/PEG30/IL70	90	82	1000	10	[11]
PVA gel	175	91	100	0.5	[13]
ZA-HGPE	230.5	83.8	150	0.2	[14]
PCZ-gel	275.1	92	200	0.5	[15]
PMC gel	270.7	71.1	500	1	[16]
3D-PAM/Ti-MXene	60	82	500	0.2	[17]
1.0 M Zn-Eutectic-SPE	**259**	**87**	**30**	**1**	**Present work**
	94	**83**	**1000**	**10**	

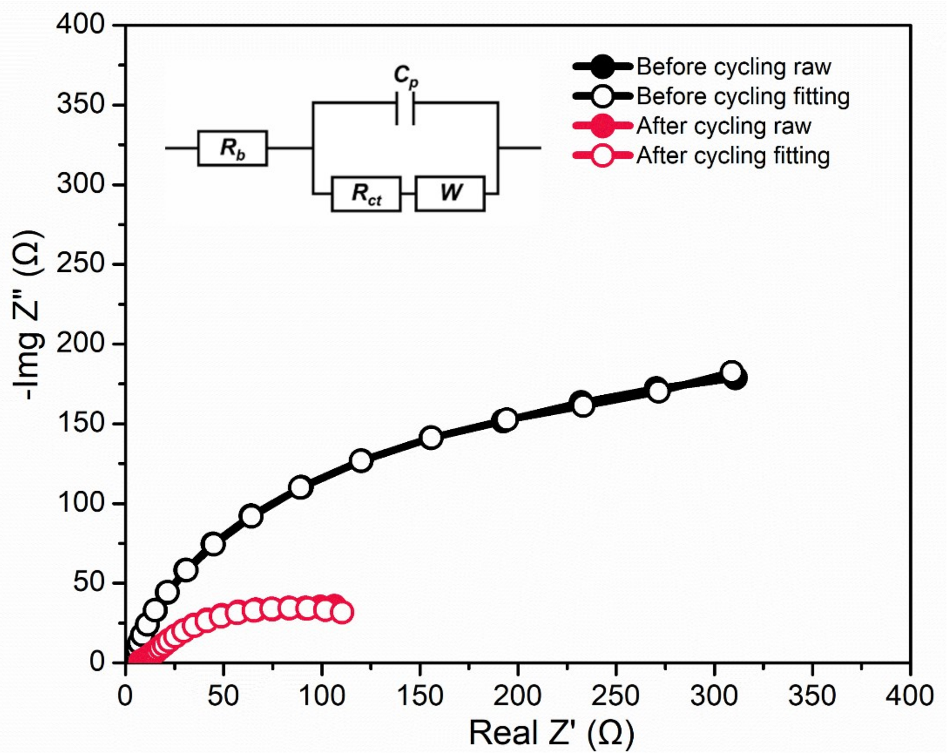

Figure S15. EIS spectra of Zn|SPE|$V_{10}O_{24}\cdot nH_2O$@rGO cell before and after the 300th cycle at 1.0 A g^{-1}.

Table S4. Bulk resistance (R_b) and charge transfer resistance (R_{ct}) values before cycling and after the 300th cycle obtained from EIS fitting.

	R_b (Ω)	R_{ct} (Ω)
Before cycling	4.50	302
After 300th cycle	7.74	154

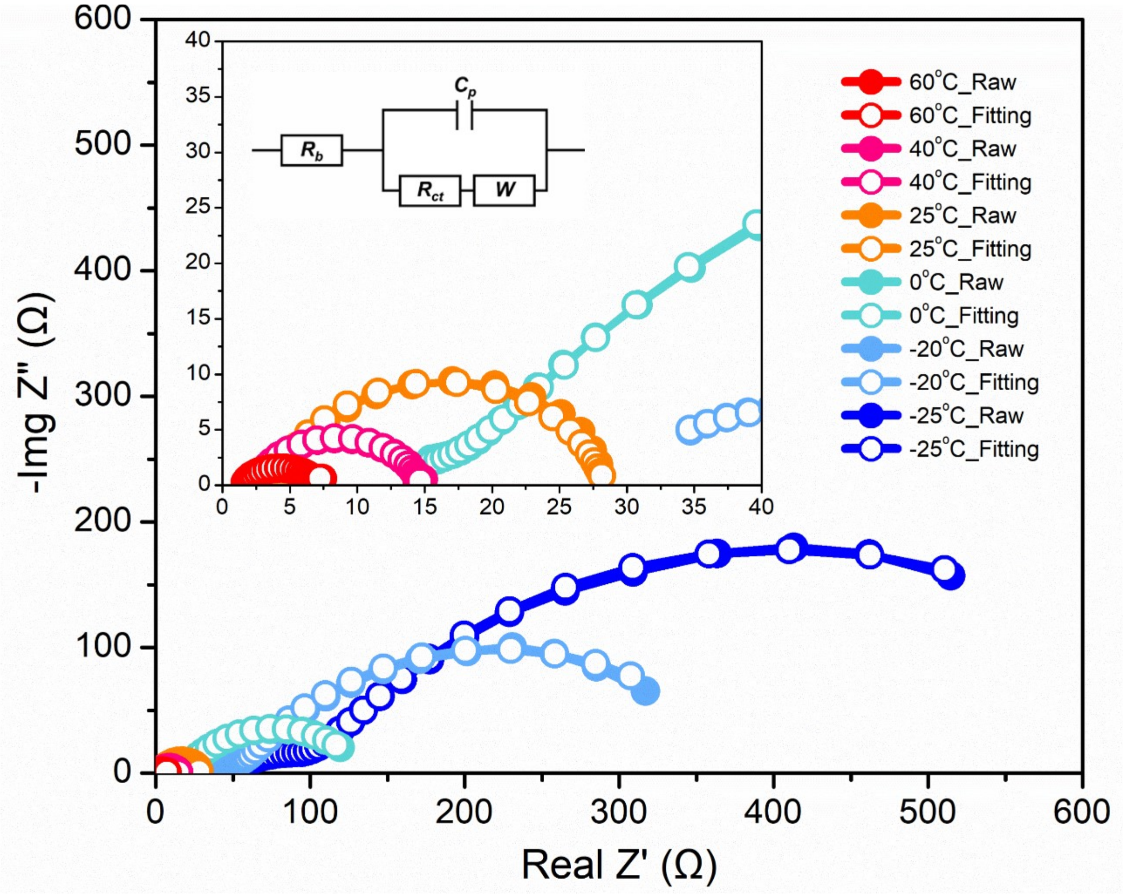

Figure S16. EIS spectra of Zn|SPE|$V_{10}O_{24}\cdot nH_2O$@rGO cell at various temperature.

Table S5. The bulk resistance (R_b) and charge transfer resistance (R_{ct}) of Zn|SPE|$V_{10}O_{24}\cdot nH_2O$@rGO cell at various temperatures.

	60 °C	40 °C	RT	0 °C	-20 °C	-25 °C
R_b (Ω)	1.5	2.4	4.0	15.4	34.7	47.5
R_{ct} (Ω)	5.4	12.4	24.4	110	343	603

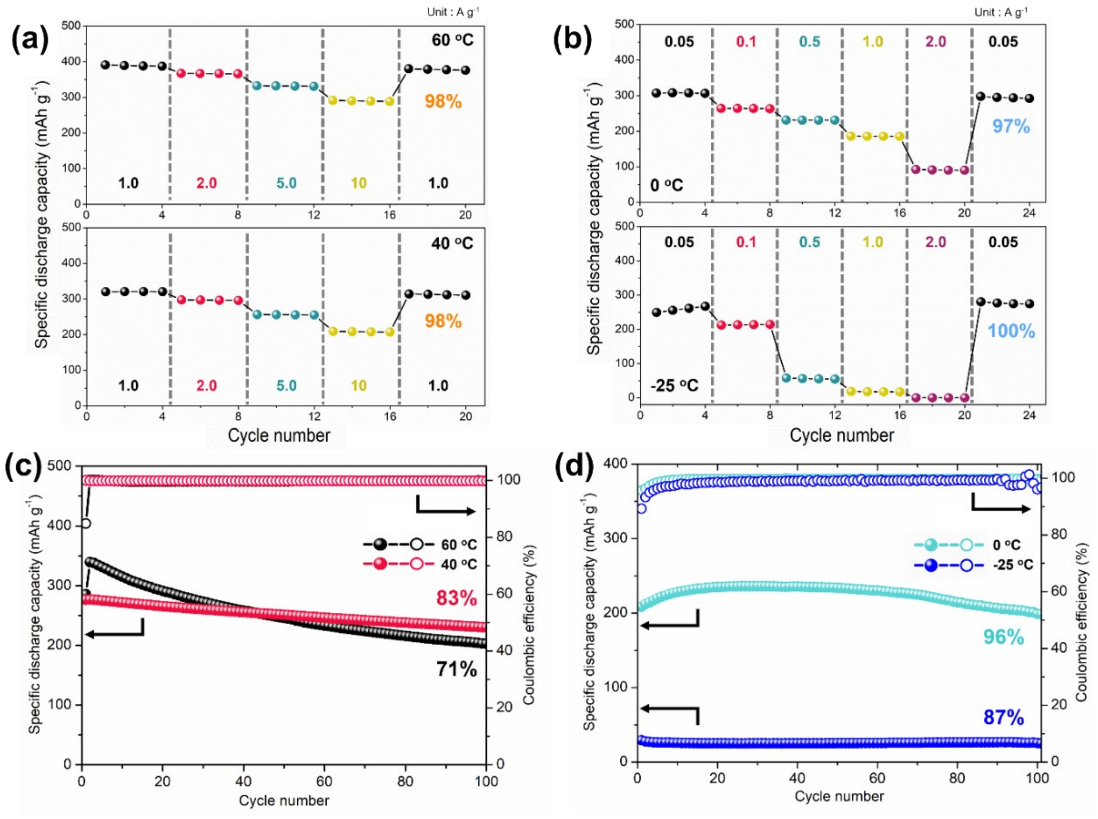

Figure S17. Electrochemical performance of Zn|SPE|$V_{10}O_{24}.nH_2O$@rGO cell: rate capability at (a) 60 and 40 °C and (b) 0 and -25 °C. Long-term cycling performance over 100 cycles at 1.0 A g^{-1}: at (c) 60 and 40 °C and at (d) 0 and -25 °C.

Table S6. Specific discharge capacities at various temperatures (60, 40, 25, 0, -20, and -25 °C) under different current densities.

Current density (A g^{-1})	**Specific discharge capacity (mAh g^{-1})**					
	60 °C	**40 °C**	**RT**	**0 °C**	**-20 °C**	**-25 °C**
0.05	-	-	-	306.7	277.7	267.3
0.1	-	-	-	263.5	241.3	214.4
0.5	-	-	-	231.0	160.7	54.7
1.0	387.3	320.4	306.4	185.5	108.8	17.3
2.0	366.1	296.0	279.5	90.3	63.2	0.05
5.0	331.3	255.1	233.3	-	-	-
10.0	288.7	207.2	183.9	-	-	-

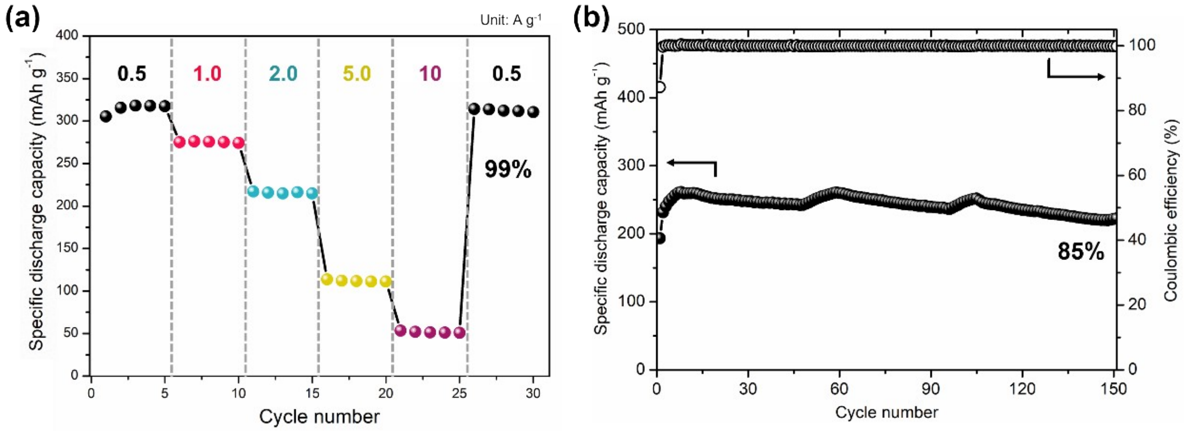

Figure S18. Electrochemical performance of Zn|SPE|$V_{10}O_{24}\cdot nH_2O$@rGO cell with mass loading of 3.0 mg cm^{-2}: (a) rate capability at different current densities (0.5-10.0 A g^{-1}) and (b) cycling performance at 1.0 A g^{-1} over 150 cycles.

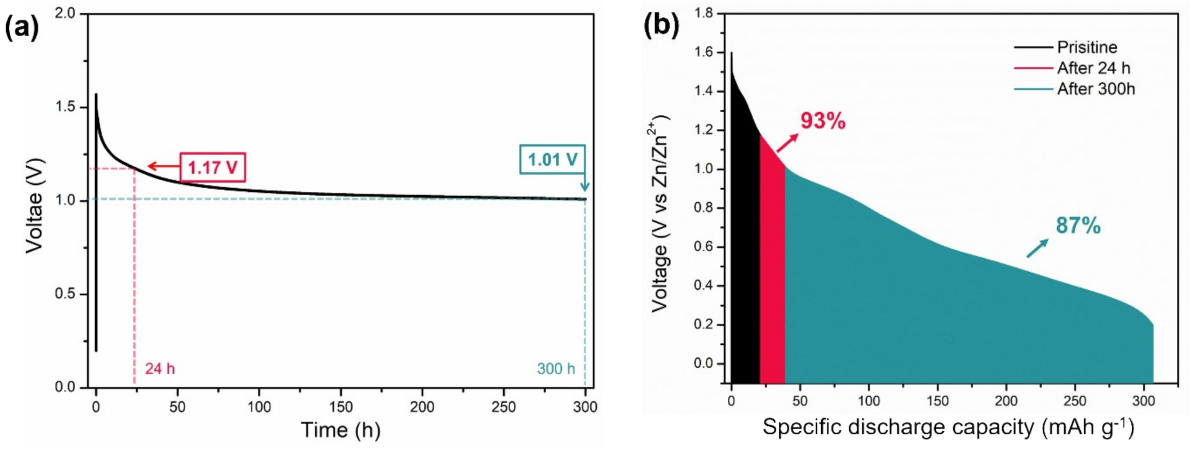

Figure S19. (a) Time-dependent self-discharge characteristic. (b) Comparison of capacity retention after 24 h and 300 h based on remaining voltage following full charge.

Reference

[1] Q. Li, T. Wei, K. Ma, G. Yang, C. Wang, Boosting the Cyclic Stability of Aqueous Zinc-Ion Battery Based on Al-Doped $V_{10}O_{24}\cdot 12H_2O$ Cathode Materials, ACS Applied Materials & Interfaces, 2019, 11, 20888-20894.

[2] L. Zhang, J. Luo, X. Bai, L. Yu, M. Wang, G. Zhao, N. Zhang, A Poly(ethylene carbonate)-based all solid state zinc ion battery, Electrochim. Acta, 2023, 470, 143336.

[3] D. Liu, Z. Tang, L. Luo, W. Yang, Y. Liu, Z. Shen, X. Fan, Self-Healing Solid Polymer Electrolyte with High Ion Conductivity and Super Stretchability for All-Solid Zinc-Ion Batteries, ACS Appl. Mater. Interfaces, 2021, 13, 36320-36329.

[4] X. Zhu, C. Ji, Q. Meng, H. Mi, Q. Yang, Z. Li, N. Yang, J. Qiu, Freeze-Tolerant Hydrogel Electrolyte with High Strength for Stable Operation of Flexible Zinc-Ion Hybrid Supercapacitors, Small, 2022, 18, 2200055.

[5] L. Zhang, J. Wu, T. Lu, X. Li, H. Wu, T. Chen, Y. Zhang, J. Wei, M. Hu, X. Zheng, H. Gao, Z. Huang, Q. Wang, S. Wang, Z. Jin, Improving Zn^{2+} migration via designing multiple zincophilic polymer electrolyte for advanced aqueous zinc ion batteries, Chem. Eng. J., 2024, 496, 153815.

[6] C. Fu, Y. Wang, C. Lu, S. Zhou, Q. He, Y. Hu, M. Feng, Y. Wan, J. Lin, Y. Zhang, A. Pan, Modulation of hydrogel electrolyte enabling stable zinc metal anode, Energy Storage Mater., 2022, 51, 588-598.

[7] H. Xia, G. Xu, X. Cao, C. Miao, H. Zhang, P. Chen, Y. Zhou, W. Zhang, Z. Sun, Single-Ion-Conducting Hydrogel Electrolytes Based on Slide-Ring Pseudo-Polyrotaxane for Ultralong-Cycling Flexible Zinc-Ion Batteries, Adv. Mater., 2023, 35, 2301996.

[8] J. Feng, D. Ma, K. Ouyang, M. Yang, Y. Wang, J. Qiu, T. Chen, J. Zhao, B. Yong, Y. Xie, H. Mi, L. Sun, C. He, P. Zhang, Multifunctional MXene-Bonded Transport Network

Embedded in Polymer Electrolyte Enables High-Rate and Stable Solid-State Zinc Metal Batteries, Adv. Funct. Mater., 2022, 32, 2207909.

[9] H. Lu, J. Hu, L. Wang, J. Li, X. Ma, Z. Zhu, H. Li, Y. Zhao, Y. Li, J. Zhao, B. Xu, Multi-Component Crosslinked Hydrogel Electrolyte toward Dendrite-Free Aqueous Zn Ion Batteries with High Temperature Adaptability, Adv. Funct. Mater., 2022, 32, 2112540.

[10] H. Li, Y. Liu, Z. Chen, Y. Yang, T. Lv, T. Chen, High voltage and healing flexible zinc ion battery based on ionogel electrolyte, J. Colloid. Interface Sci., 2023, 639, 408-415.

[11] R. Puttaswamy, Z. Tian, H. Lee, D.Y. Kim, A. L. Mong, D. Kim, High-performance solid-state zinc-ion batteries enabled by flexible and highly Zn^{2+} conductive solid-polymer electrolyte, J. Mater. Chem. A, 2023, 11, 14075-14085.

[12] Z. Chen, X. Li, D. Wang, Q. Yang, L. Ma, Z. Huang, G. Liang, A. Chen, Y. Guo, B. Dong, X. Huang, C. Yang, C. Zhi, Grafted MXene/polymer electrolyte for high performance solid zinc batteries with enhanced shelf life at low/high temperatures, Energy Environ. Sci., 2021, 14, 3492-3501.

[13] B. Sun, Y. Zong, K. Bao, M. Wang, P. Wang, H. Xu, Y. Jin, Activating Gel Polymer Electrolyte Based Zinc-Ion Conduction with Filler-Integration for Advanced Zinc Batteries, ACS Appl. Mater. Interfaces, 2023, 15, 37916-37924.

[14] Z. Zheng, H. Cao, W. Shi, C. She, X. Zhou, L. Liu, Y. Zhu, Low-Cost Zinc–Alginate-Based Hydrogel–Polymer Electrolytes for Dendrite-Free Zinc-Ion Batteries with High Performances and Prolonged Lifetimes, Polymers, 2023, 15, 212.

[15] H. Zhang, X. Gan, Z. Song, J. Zhou, Amphoteric Cellulose-Based Double-Network Hydrogel Electrolyte Toward Ultra-Stable Zn Anode, Angew. Chem. Int. Ed., 2023, 62, e202217833.

[16] P. Lin, J. Cong, J. Li, M. Zhang, P. Lai, J. Zeng, Y. Yang, J. Zhao, Achieving ultra-long lifespan Zn metal anodes by manipulating desolvation effect and Zn deposition orientation in a multiple cross-linked hydrogel electrolyte, Energy Storage Mater., 2022, 49, 172-180.

[17] A. C. Radjendirane, F. M. Sha, B. Balan, S. Ramakrishnan, K. Vediappan, S. P. Rajendra, M. S. Alsalhi, S. Angaiah, 3D-Polyacrylamide/Ti-MXene: A Newer Hybrid Hydrogel Electrolyte Featuring High Mechanical Strength and Durability for Flexible Aqueous Zinc-Ion Batteries, ACS Appl. Energy Mater, 2024, 7, 4745-4760.